



Preparation and photocatalytic activity of Mo-modified Ti-doped HAp

Noppakhate Jiraborvornpongsa^a, Toshihiro Isobe^a, Sachiko Matsushita^a, Mitsutake Oshikiri^b,
Masato Wakamura^c, Kotaro Fujii^d, Masatomo Yashima^d, Akira Nakajima^{a,*}



^a Department of Materials Science and Engineering, School of Materials and Chemical Technology, Tokyo Institute of Technology, 2-12-1 O-Okayama, Meguro, Tokyo 152-8552, Japan

^b International Center for Materials Nanoarchitectonics (WPI-MANA), National Institute for Materials Science (NIMS), 3-13 Sakura, Ibaraki 305-0003, Japan

^c Device & Materials Laboratory, Fujitsu Laboratories Ltd., 10-1 Morinosato-Wakamiya, Atsugi, Kanagawa 243-0197, Japan

^d Department of Chemistry, School of Science, Tokyo Institute of Technology, 2-12-1 O-Okayama, Meguro, Tokyo 152-8551, Japan

ARTICLE INFO

Keywords:
Hydroxyapatite
Photocatalyst
Mo
Ti
Modification

ABSTRACT

Titanium-doped hydroxyapatite (Ti-HAp, $(\text{Ca}_{10-2x}, \text{Ti}_x, \square_x)(\text{PO}_4)_6(\text{OH})_2$, \square : defect in Ca site) powders were modified with a CaMoO_4 aqueous solution. Then their photocatalytic activity under UV illumination was evaluated by the decomposition of gaseous 2-propanol. The crystal structure, morphology, light absorption, and specific surface area were almost unchanged by the modification, but small clusters were deposited onto the Ti-HAp surface. The photocatalytic activity of the Mo-modified samples increased concomitantly with increasing Mo concentration until 0.5% against Ti. The highest photocatalytic activity of Mo-modified Ti-HAp was about nine times higher than that of Ti-HAp. Computer modeling revealed that the contribution of MoO_4^{2-} doping into the Ti-HAp structure plays no important role in the activity increase. A Mo(V) signal appeared by UV illumination in electron spin resonance spectra of Mo-modified Ti-HAp. The Mo modification decreased the photoluminescence intensity. These results suggest that photoinduced electrons can transfer from the Ti-hybridized band to the cluster, thereby improving the carrier separation efficiency and engendering higher photocatalytic activity.

1. Introduction

Hydroxyapatite (HAp, $\text{Ca}_{10}(\text{PO}_4)_6(\text{OH})_2$) is a major component of biological hard tissues because of its good affinity against proteins. Therefore, synthetic HAp has been used widely for various applications as adsorbents, artificial bones and teeth, ion exchangers, and catalysts [1–4]. Moreover, previous reports have described that HAp shows good photo-oxidation ability against methyl mercaptane and dimethyl sulfide under the illumination of deep UV light ($\lambda = 254$ nm) [5–7]. The Ca ion in the structure of HAp is exchanged easily with other cations [8,9]. When Ca is substituted with Ti, a hybridized band of Ti 3d and O 2p orbitals is created between the bandgap of HAp [10]. Then, the titanium-substituted hydroxyapatite (Ti-HAp, $(\text{Ca}_{10-2x}, \text{Ti}_x, \square_x)(\text{PO}_4)_6(\text{OH})_2$, \square : defect in Ca site) possesses photocatalytic activity under UV illumination while retaining surface chemical properties of HAp [11–18]. Consequently, Ti-HAp exhibits good affinity with organic compounds. That affinity gives it characteristically higher adsorption capability than other normal oxides against various organic chemical species [13,14]. For that reason, Ti-HAp is highly anticipated for anti-bacterial applications [17,18]. Recently, this property was reported as

attainable on strontium hydroxyapatite [19].

The maximum substitutable Ti amount is limited to ca. 10 mol% of Ca to retain the HAp structure. Therefore, the photocatalytic activity of Ti-HAp itself is restricted [11]. Consequently, the primary photocatalytic activity of Ti-HAp is inferior to that of TiO_2 . The high photocatalytic activity of Ti-HAp against various organic compounds is attributable to its excellent adsorption capability on their surface [20]. The enhancement of primary photocatalytic activity of Ti-HAp is demanding. Several attempts have been conducted. Wakamura et al. modified Cr(III) onto Ti-HAp and enhanced photocatalytic activity under visible light [21]. However, the visible light absorption was insufficient for practical use. Nishikawa et al. reported grafting of Cu(II) ions onto Ti-HAp [22]. In their work, the photocatalytic activity for the decomposition of gaseous acetaldehyde under UV illumination was increased because of electron transfer to Cu(II) via the Ti-hybridized band, which promotes carrier separation. However, photocatalytic activity improvement by this method was, at most, three times that of pure Ti-HAp. The contribution of interfacial charge transfer absorption by Cu ion, which is commonly used for imparting visible light photocatalytic activity to TiO_2 [23,24], was scarce. Enhancement of the

* Corresponding author.

E-mail address: anakajim@ceram.titech.ac.jp (A. Nakajima).

primary photocatalytic activity of Ti-HAp has not been achieved to date.

In contrast, MoO_4^{2-} is a tetrahedral oxoanion that is similar in many respects to PO_4^{3-} . Although ion exchange between MoO_4^{2-} and PO_4^{3-} in Ti-HAp is expected to be difficult because of their sizes ($\text{P} = \text{O}$, ca. 150 pm; $\text{P}-\text{O}$, ca. 160 pm; $\text{Mo}-\text{O}$, ca. 170 pm [25,26]), MoO_4^{2-} might adsorb onto the surface Ca or Ti ion, where it might affect the charge transfer of the material. For this study, we modified Ti-HAp using an aqueous solution of CaMoO_4 to avoid unnecessary ion exchange of the Ca sites in Ti-HAp. Then we examined the photocatalytic activity under UV illumination and discussed the role of Mo modification in photocatalytic activity.

2. Experimental

2.1. Sample preparation and characterization

For this study, commercial Ti-HAp (Hautoform TA, $(\text{Ca}_{0.22}, \text{Ti}_{0.89}, \square_{0.89})(\text{PO}_4)_6(\text{OH})_2$; Fuji Chemical Ind. Co. Ltd., Osaka, Japan) was used as a starting material. Reagent grade calcium molybdate (CaMoO_4 ; Wako Pure Chemical Industries Ltd., Osaka, Japan) was dissolved into distilled water (200 mL, 0.1 mM) at 80 °C. After cooling the solution to room temperature, Ti-HAp powder (1 g) was added to the clear CaMoO_4 solution and was stirred for 5 min. The powder was filtered and washed several times with distilled water. Then, the powder was dried at 60 °C for 24 h in air, followed by heating at 500 °C for 1 h in ambient air. This firing was conducted to remove organic compounds and to convert hydroxides to oxides. This temperature was lower than the heating temperature in manufacturing commercial Ti-HAp process. For that reason, it will not provide a remarkable difference in the crystalline phase, morphology, or specific surface area of the starting Ti-HAp. These procedures were repeated several times (X) to control the chemical composition of the surface. The obtained samples are denoted in this report as CM-X. We also prepared samples for comparison using HAp (Taihei Chemical Industrial Co. Ltd., Osaka, Japan) instead of Ti-HAp.

Crystalline phases of the obtained samples were investigated using X-ray diffraction (XRD; XRD-6100, Shimadzu Corp., Japan) with $\text{Cu K}\alpha$ radiation. The optical absorption spectra were measured using a UV-vis scanning spectrophotometer (V-650; Jasco Corp., Tokyo, Japan). The powder morphology was observed using a transmission electron microscope (JEM-2010 F; JEOL Ltd., Tokyo, Japan). We evaluated the chemical composition using inductively coupled plasma analysis (Prodigy ICP; Teledyne - Leeman Labs, Hudson, NH, U.S.A.). Additionally, we measured the binding energies of the elements using X-ray photoelectron spectroscopy (XPS, ESCA model 5500MT; PerkinElmer Inc., U.S.A.) using an $\text{Al K}\alpha$ X-ray line (1486.6 eV). Specific surface areas were measured using Brunauer, Emmett and Teller (BET) method with N_2 (BEL SORP mini; Bel Japan Inc., Japan).

2.2. Photocatalytic activity, electron spin resonance, and photoluminescence measurements

Photocatalytic activity was evaluated according to the decomposition of gaseous 2-propanol (IPA). The powder samples (40 mg) are embedded homogeneously into a petri dish with area of 8.35 cm^2 . Before evaluation, UV pre-illumination (ca. 0.7 mW/cm² at 365 nm) onto the sample powder was conducted for one night (more than 8 h) to remove organic compounds that had been adsorbed onto the surface. Then the dish was set at the center of a Pyrex glass vessel with a quartz lid (500 mL in volume). Subsequently, the vessel was sealed, followed by filling of the vessel with air (20 °C, 80% RH). Then, 700 ppm of gaseous IPA was injected into the vessel. It was then stored in the dark. During this dark storage, the IPA concentration was evaluated using gas chromatography (GC-2014 with a flame ionization detector, a methanizer, and a column (Sunpak-A; Shimadzu Corp.); Shimadzu Corp.,

Tokyo, Japan) to confirm the adsorption equilibrium between the powder and gaseous IPA. After the adsorption equilibrium was confirmed (one night), light illumination was conducted. Then we applied UV illumination using a UV illuminator (LA-410UV-1; Hayashi Watch Works, Tokyo, Japan) equipped with a Hg-Xe lamp through a liquid light guide with no filter. The UV illumination intensity was adjusted to 1 mW/cm². During this light illumination, IPA and CO_2 concentrations were measured every 1 h using the same gas chromatography. A schematic illustration of photocatalytic activity measurements and the light source spectra are presented in Fig. S1 in Supporting Information.

For electron spin resonance (ESR) measurements, the sample powder was placed in a quartz glass sample tube with a Young vacuum joint and a stopcock. Then the air was evacuated from the sample tube. Measurements were taken at 90–100 K using an ESR spectrometer (EMXnano; Bruker Analytik, Germany) under light using a UV illuminator (LA-410UV-1; Hayashi Watch Works, Tokyo, Japan) equipped with a 200 W Hg-Xe lamp. The ESR measurement conditions were microwave frequency of 9.62 GHz, microwave power of 1 mW, and field modulation of 0.05 mT. The photoluminescence (PL) emission spectra were measured using a fluorescence spectrophotometer (F-7100; Hitachi Ltd., Japan) with a 150 W Xe lamp as an excitation light source. The excitation wavelength was 280 nm. The scanning rate was 1200 nm/min. The PMT voltage was 700 V. Widths of excitation emission slits were 5.0 nm.

2.3. Density functional theory calculation

To elucidate the role of the Mo-modified Ti-HAp, we specifically examined a room-temperature equilibrated system and its related electronic structure. Ti-HAp has the $P6_3/m$ space group (No. 176), with the lattice parameter and bond angle defined respectively as $a = b = 9.4212 \text{ \AA}$, $c = 6.8847 \text{ \AA}$, $\alpha = \beta = 90^\circ$, and $\gamma = 120^\circ$. The photocatalytic system was modeled by placing the Mo-modified Ti-HAp slab substrate in a supercell. The exposed surface of the Mo-modified Ti-HAp was selected as the (001) surface. The supercell contained the photocatalyst substrate composed of 1 Mo, 8 Ti, 72 Ca, 47 P, 225 O, and 33 H atoms with 16 Mo atoms forming a metallic cluster added to the surface. The exposed surface area on the slab was $2a \times 2b \times \sin(120^\circ)$ ($= 307.47 \text{ \AA}^2$). The supercell thickness was set as 25.0 \AA , whereas the slab representing the substrate occupied about $2c$ (13.7694 \AA) of the total supercell thickness. The remaining empty space is available to accommodate the Mo metallic cluster, 2-propanol (IPA), oxygen, and nitrogen. Then the structure equilibrated to 300 K was obtained by dynamic simulation within the Car-Parrinello Molecular Dynamic (CPMD) framework [27] by exposing the model to 300 K conditions for about 0.64 ps. The electronic structure of the Mo-modified Ti-HAp was obtained by solving a Kohn-Sham equation with local spin density approximation using first-principles method.

3. Results and discussion

3.1. Characteristics of obtained samples

Fig. 1 presents XRD patterns of Ti-HAp before and after Mo modification. All peaks in the XRD patterns of the obtained samples were identified as a HAp structure with $P6_3/m$ (No.176) space group. Differences in intensity among the peaks before and after the Mo modification were not remarkable. The specific surface areas of all samples were almost equivalent (35–39 m^2/g).

Fig. 2 portrays TEM images of Ti-HAp obtained before and after three Mo modifications (CM-3). Both samples have rod-like morphology with 50 nm average particle length. A cluster-like area with size of 1–2 nm was observed on the CM-3 powder surface (denoted by circles and arrows in Fig. 2(b) and (c)). However, analysis of the chemical compositions of these parts using EDS was not feasible because of insufficient durability against damage by the focused electron beam.

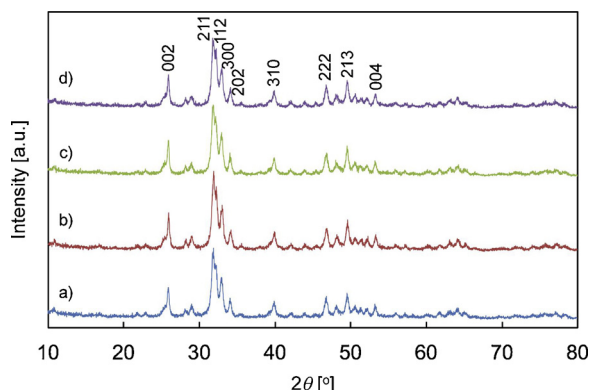


Fig. 1. XRD patterns of sample powders: (a) Ti-HAp, (b) CM-1, (c) CM-3, and (d) CM-5.

Based on the processing procedures, the chemical composition (described below), and their morphology, it was inferred that clusters observed in TEM were CaMoO_4 or MoO_x .

Fig. 3 presents UV-vis spectra of Ti-HAp before and after Mo modification. No absorption band except for the absorption band of Ti-HAp was observed. It is noteworthy that the absorption edge of crystalline CaMoO_4 is on the smaller wavelength side than that of Ti-HAp (see Fig. S2 in Supporting Information). The bandgaps of the samples calculated from UV-vis spectra by assuming direct transition were 3.72 eV for all samples, which were approximately equal to the reported values for Ti-HAp [10,16]. Detailed inspection of the valence band (O 2p) top of Ti-HAp and CM-5 obtained by XPS revealed that they are more positive (0.480 eV) against those of TiO_2 , as shown in Fig. S3 in Supporting Information, for which the band position was clarified in our earlier study [28]. Therefore, the valence band position of Ti-HAp was estimated from the bandgap energy as 3.560 V (vs. NHE, pH = 0); the Ti-hybridized band was estimated as approximately -0.160 V (vs. NHE, pH = 0).

Table 1 presents chemical compositions obtained from ICP analysis. At first, we conducted XPS analysis for the Mo characterization. However, because of the very low concentration, the peak intensity against the background noise level was insufficient. Reliable elucidation related to the amount and valence was infeasible. Therefore, we confirmed Mo concentration using ICP analysis in this study. For the peak of Ti 2p and O 1s, no change was found after Mo modification. The Mo concentration in the table was the atomic ratio against Ti in Ti-HAp. It is noteworthy that the atomic ratio between Ca and Ti (Ca/Ti) was almost constant (9.1 ~ 9.4) in these samples. The concentration of Mo increased concomitantly with increasing modification time up to three times the original concentration. Subsequently, the concentration of Mo decreased gradually, which might indicate that the excessive amount of Mo or Ti-HAp surface dissolved into the CaMoO_4 solution. Some

molybdenum oxides possess a certain solubility against water (ca. 0.5 g/100 mL water at 300 K for MoO_3). Therefore, the cluster might dissolve into water if it is MoO_x . However, to date, we have insufficient confidence about the reason for the Mo concentration presented in Table 1. Investigation of the effects of the impregnation time period might provide some information. This work will be addressed in future studies.

3.2. Photocatalytic activity

Figs. 4(a) and (b), respectively portray the concentration change of IPA and CO_2 against the UV illumination time. The value of C_0 presented on the y-axis of Fig. 4(a) shows the initial concentration of IPA before UV illumination. The practical average value of C_0 is around 622 ppm. The IPA concentration reaches zero within 6 h for Ti-HAp, within 3 h for CM-1, and within 2 h for the remaining samples. Although little difference was observed among CM-2 to CM-5, the CO_2 generation rates of these samples differed because several steps exist in the decomposition pathway from IPA to CO_2 by photocatalytic oxidation [29–32]. Table 1 shows that the CO_2 generation rate (K_{CO_2}) at the initial stage was calculated in the linear range of 0–6 h of the relation between the CO_2 generation and the UV illumination time. The highest CO_2 generation rate of the Mo-modified Ti-HAp (131 ppm/h) was about nine times higher than that of Ti-HAp (14 ppm/h). Fig. 5 presents the relation between the Mo amount and the CO_2 generation rate. From this relation, the photocatalytic activity under UV illumination of the Mo-modified Ti-HAp was found to be enhanced as the Mo concentration increased. Figure S4 presented in Supporting Information shows that this photocatalytic activity was not degraded significantly through at least three repeated measurements. Although the degree of activity increase was less remarkable (5 times) than IPA, similar trend was obtained also on the decomposition of acetaldehyde (Fig. S5 in Supporting Information) under the same condition. This difference should be attributable to the difference in adsorption capability against gaseous species and their decomposition pathway [33].

Further detailed experimentation revealed that Mo-modified HAp (specific surface area of ca. $29 \text{ m}^2/\text{g}$) prepared using the same procedures as those used for Mo-modified Ti-HAp exhibit little absorption in UV-vis spectra and decomposition activity (see Figs. S6 and S7 in Supporting Information). These results imply that Mo modified using this treatment does not provide photocatalytic activity by itself, but that it efficiently enhances the photocatalytic activity of Ti-HAp under UV illumination.

For computer modeling, we specifically examined the structure of Mo-modified Ti-HAp with a 16-atom Mo cluster placed on the surface. In a bulk metallic state, Mo crystallizes in the form of a body-centered cubic structure belonging to the space group $Im\bar{3}m$ (No. 229). The reported unit cell lattice constant is 3.1461 Å, the shortest Mo–Mo distance being 2.7246 Å [34]. For the Ti-HAp structure, Ca atoms were substituted with Ti atoms in both the Ca(I) site and Ca(II) site at 10 mol

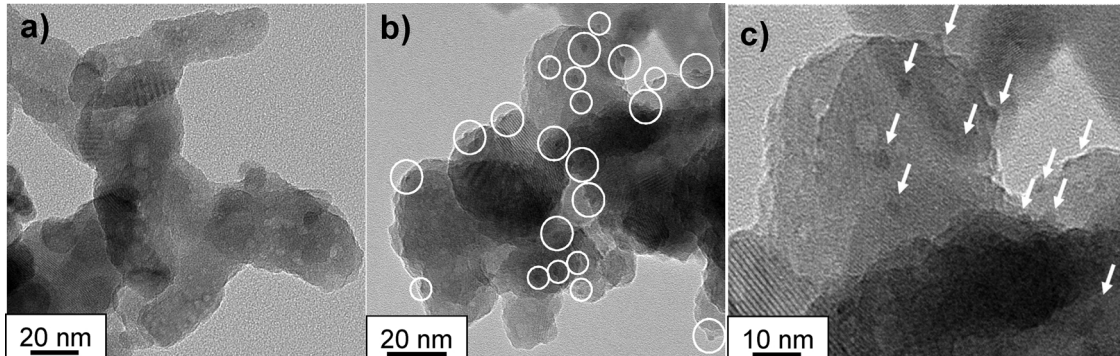


Fig. 2. TEM micrographs of Ti-HAp particles: (a) before Mo modification, and (b) and (c) after Mo modification (sample: CM-3).

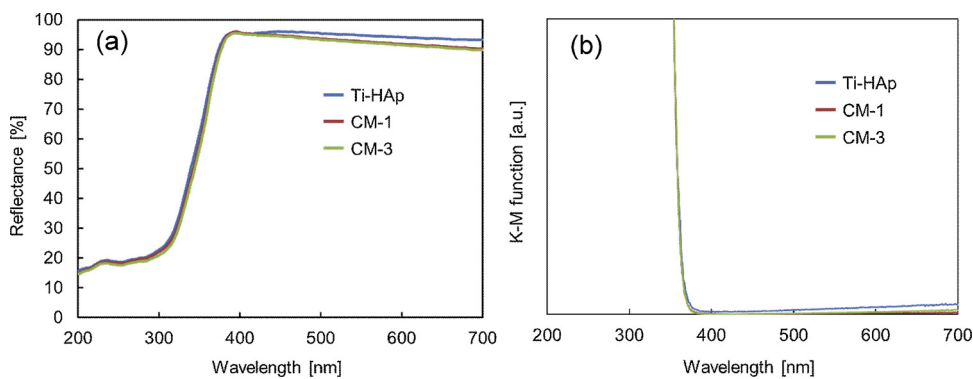


Fig. 3. UV-vis spectra (a) and Kubelka-Munk function plots (b) of Ti-HAp, CM-1, and CM-3.

Table 1

Chemical compositions obtained from ICP analysis and the CO_2 generation rate.

Sample name	Mo/Ti [mol%]	K_{CO_2} [ppm/h]
Ti-HAp	–	14
CM-1	0.16	44
CM-2	0.33	82
CM-3	1.21	112
CM-4	1.10	121
CM-5	0.91	121
CM-6	0.64	123
CM-7	0.50	131
CM-8	0.46	121

% of Ca atoms [10]. In addition, one unit of tetrahedral PO_4^{3-} was substituted with tetrahedral MoO_4^{2-} in the Ti-HAp structure. When the simulation approaches thermal equilibrium, the Mo cluster displaces closer to the O atom at the surface. Eventually, Mo atoms of the cluster are adsorbed to O atoms of Ti-HAp, forming a stable Mo-O oscillating dynamically around 2.16 Å [35] and keeping the Mo cluster anchored to the surface. The initial shape of the Mo cluster changed, accompanied by shrinkage of the Mo–Mo distance from 2.7 Å to about 2.3–2.7 Å. Details of the electronic properties were investigated for the equilibrated system. Fig. 6 presents the atomic configuration of the surface in the system

A projection of eigenwavefunction onto atomic orbitals produced the result presented in Fig. 7. The conduction band comprises Ca 4s orbitals, whereas the lowest unoccupied band is composed predominantly by Ti 3d and Mo 4d contributions. Fig. 7(d) portrays the occupied states of Mo 4d orbitals, which are situated in the energy range from the O 2p band to the middle of Ti-HAp band gap energy. From these energy band levels, one can infer that an electron can be feasibly excited from the valence band (O 2p orbitals) to the Ti 3d

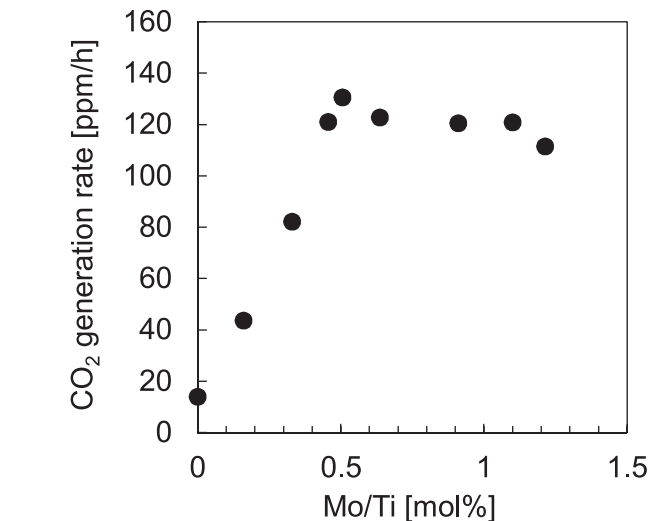


Fig. 5. Relation between the Mo concentrations and the CO_2 generation rates of all samples.

unoccupied band, which is hybridized with the unoccupied Mo 4d band then transferred to Mo 4d orbitals of the Mo metallic cluster. Therefore, the excited electron is separated from the hole in the valence band, providing carrier separation [36].

Among the Mo 4d components, two positions of Mo atoms exist in this system. The first position is a Mo atom forming MoO_4^{2-} tetrahedral that substituted with PO_4^{3-} tetrahedral in Ti-HAp structure. The second position is Mo atoms forming the Mo metallic cluster. Fig. 7(g) and (h) respectively present the contributions of Mo 4d orbitals of Mo1, which is located inside the Ti-HAp slab layer as MoO_4^{2-} tetrahedral

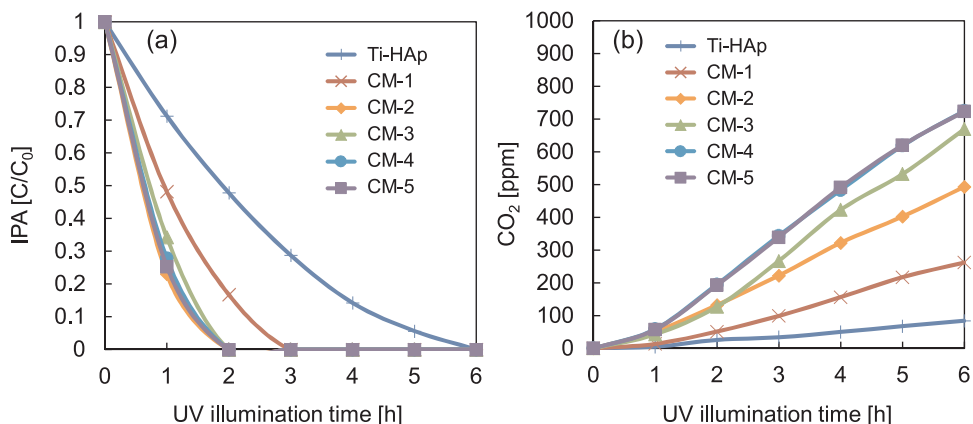
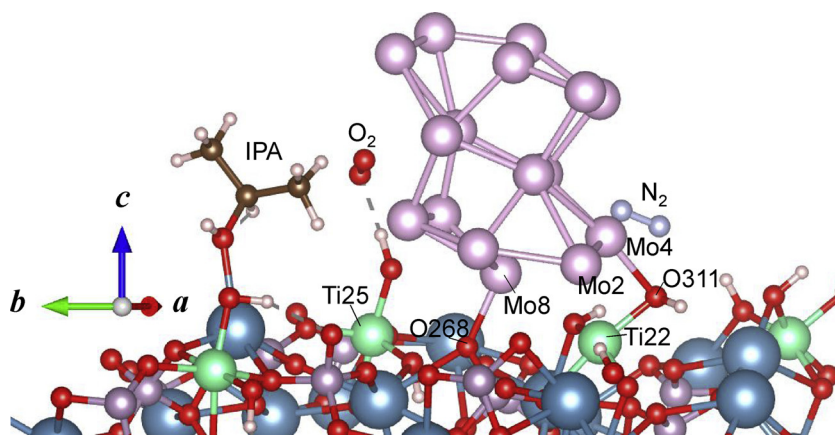


Fig. 4. Concentration changes of (a) gaseous IPA and (b) CO_2 against UV illumination time.



structure, and Mo4, which is on the Mo metallic cluster. The Mo 4d components of Mo1 are located only in the unoccupied state from -0.8 to 3.0 eV. However, the Mo 4d components of Mo4, which represent all 4d components of the metallic Mo cluster (Fig. 7(d)), are located in the energy range of -4.0 to 3.0 eV, indicating that only the Mo atoms forming the Mo metallic cluster are involved in the increase of photocatalytic activity. These results suggest that Mo-doping by exchanging PO_4^{3-} with MoO_4^{2-} tetrahedral does not increase photocatalytic activity. Moreover, we can infer that an electron excited from O 2p (valence band) to Ti-Mo hybridized band can transfer to the Mo cluster. Consequently, the excited electron is separated from the hole, providing efficient carrier separation.

For this study, we specifically examined two extreme cases: Mo^{6+} (MoO_4^{2-}) and Mo^0 (Metallic) because the intermediate state can be inferred from the results. In the case of Mo^{5+} or Mo^{4+} , electrons are injected to the d-band of MoO_x . The d-levels filled by the injected electron should appear around the highest occupied level in Fig. 7 (see Fig. S8 in Supporting Information). In the case of CaMoO_4 , which includes Mo^{6+} , the electronic structure is expected to be similar to the tetrahedral MoO_4^{2-} doped into Ti-HAp, which has already been demonstrated in our simulation model by the Mo (marked by number 1) O_4 structure. Actually, the MoO_4^{2-} structure is located in the lower part in the outer range of Fig. 6. Consequently, according to this calculation, the cluster seems to be MoO_x .

Fig. 8 portrays ESR spectra and the effect of UV illumination for Ti-

Fig. 6. Atomic configuration of the Ti-HAp surface with a Mo metallic cluster and IPA adsorbed onto the surface, and O_2 and N_2 near the surface. The color code is red for O, white for H, pink for Mo, green for Ti, blue for Ca, gray for N, and brown for C (For interpretation of the references to colour in this figure legend, the reader is referred to the web version of this article).

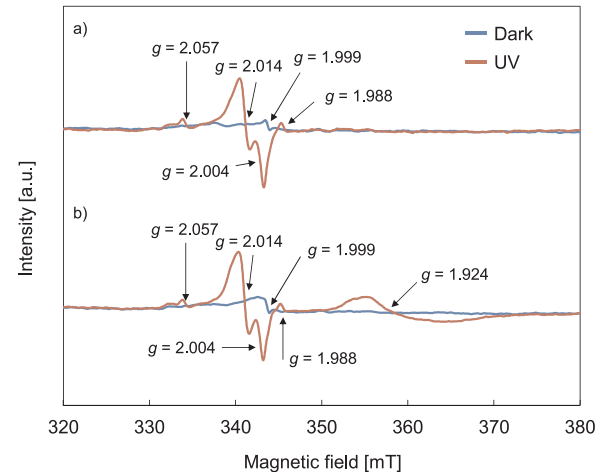


Fig. 8. ESR spectra of (a) Ti-HAp and (b) CM-3, showing the effects of UV illumination.

HAp and Mo-modified Ti-HAp (CM-3). Both samples gave the signal in the dark at 344 mT ($g = 1.999$) corresponding to that of oxygen vacancy or crystalline defects [37,38], suggesting some defects that arise from the substitution of Ti atom into the Ti-HAp structure. From UV illumination, the signal of adsorbed oxygen radical was observed at

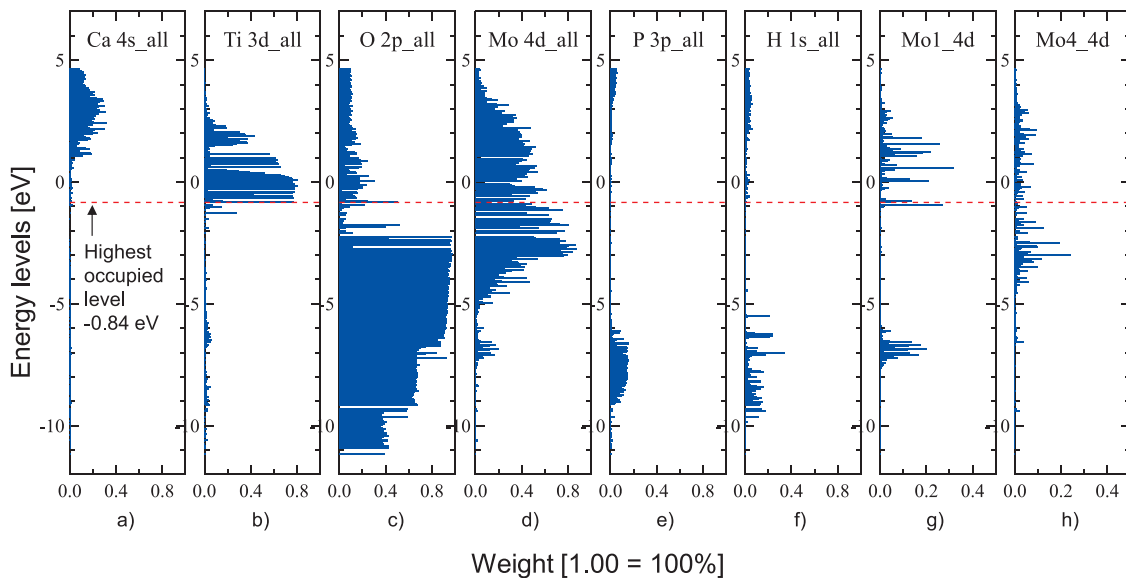


Fig. 7. Electronic structure obtained by projection onto atomic orbitals of the Mo-modified Ti-HAp at 300 K.

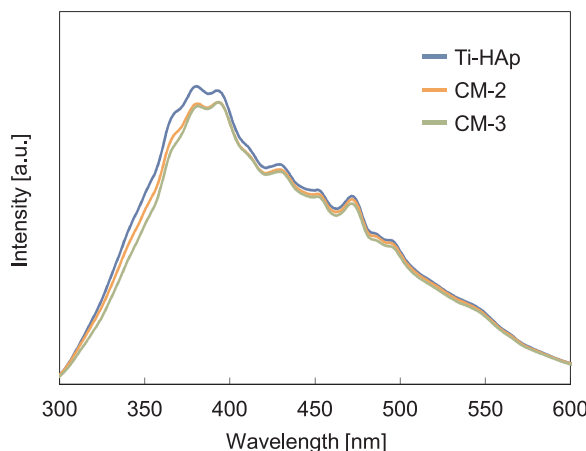


Fig. 9. PL emission spectra of Ti-HAp, CM-2, and CM-3 with excitation wavelength of 280 nm.

334 mT ($g = 2.057$) [39,40] for both samples, indicating that a slight amount of adsorbed oxygen molecules exists on the sample surface. Signals attributable to trapped holes and trapped electrons were observed respectively at 341 and 343 mT ($g = 2.014$ and 2.004) and 346 mT ($g = 1.988$) [41,42] for both samples. For the CM-3 sample, the signal of Mo(V) was observed at 358 mT ($g = 1.924$) [43] under UV illumination, as presented in Fig. 8(b). As described above, because of the quite low Mo concentration against Ti, evaluation of the valence of Mo in the cluster by XPS was not feasible. However, based on the starting materials and processing conditions (firing at 500 °C in ambient air atmosphere), one can expect that the clusters are CaMoO_4 or MoO_x and that their dominant valence should be Mo(VI). The ESR results indicate that Mo(VI) of the cluster was reduced to Mo(V) by receiving the photo-excited electrons, probably from the Ti-hybridized band. This electron transfer process provides charge separation that enhances the photocatalytic activity. It is noteworthy that this Mo(V) signal was not observed for Mo-modified HAp even under UV illumination, which means that this charge transfer is specific to Mo-modified Ti-HAp.

Fig. 9 presents the PL emission spectra of Ti-HAp and Mo-modified Ti-HAp examined at wavelengths of 300–600 nm. For all samples, the PL emission spectra appear at wavelengths of 300–590 nm. The PL emission peaks visible at wavelengths of 370–550 nm are attributable to excitonic PL, which mainly result from surface oxygen vacancies and defects of Ti-HAp particles [44,45]. Actually, Ti-HAp possesses many defects at Ca sites because of the charge compensation maintained when Ca was substituted with Ti. Therefore, the crystal defects might involve its recombination. After Mo modification, CM-2 and CM-3 showed lower PL emission intensities near the band-band PL peak (335 nm for the bandgap energy of 3.72 eV), which indicates that the recombination rate of photoinduced electron-hole pairs near the Ti-hybridized band decreased. That decrease in turn suggests that the electrons in the valence band were excited to the Ti-hybridized band. Thereafter, they migrate to the cluster, which suppresses the recombination of electron-hole pairs.

Fig. 10 presents a schematic illustration of the expected charge transfer mechanism of Mo-modified Ti-HAp. Under UV illumination, the electrons in the valence band are excited to the Ti-hybridized band. Then the excited electrons can transfer to the cluster because the potential of Ti-hybridized band ($E^\circ = -0.160$ V, vs. NHE, pH = 0) is lower than that of Mo(VI)/Mo(V) ($E^\circ = 0.400$ V, vs. NHE, pH = 0) [46] or $\text{MoO}_3/\text{MoO}_2$ ($E^\circ = 0.320$ V, vs. NHE, pH = 0) [47]. It is noteworthy that Mo(IV) is inert for ESR analysis and that Mo(V) is not stable in an ambient air atmosphere. The electrons transferred from the Ti-hybridized band to the clusters can reduce oxygen ($\text{O}_2/\text{H}_2\text{O}_2$, $E^\circ = 0.695$ V, vs. NHE, pH = 0 [48]) similarly to Cu(II)-modified TiO_2 and WO_3 [49], although photoinduced holes remain in the valence

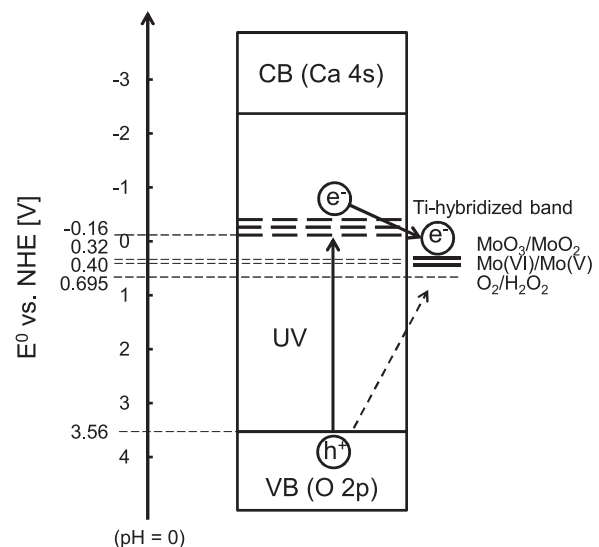


Fig. 10. Feasible charge transfer process under UV illumination of Mo-modified Ti-HAp.

band, where they can oxidize organic compounds such as IPA and acetone. This result represents one plausible explanation for the electron transfer to oxygen. Further detailed investigations must prove this pathway. However, this process suppresses recombination of the photoinduced electron-hole pairs, causing the increase in photocatalytic activity. According to the UV-vis spectra, the direct electron transfer from the valence band to the cluster via interfacial charge transfer seems unlikely to occur, probably because of the bonding nature of PO_4^{3-} , as described in an earlier report [22]. The present study revealed that 0.4–0.5 mol% is an optimum concentration for Mo modification (Fig. 5). A plausible explanation of this amount is an appropriate concentration for the balance between oxidation and reduction sites in the surface of Ti-HAp. The overall activation mechanism for Mo modification is apparently similar to the case of Cu modification [22]. However, Mo modification was more efficient than the case of Cu modification. Chemical affinity onto the Ti-HAp surface (MoO_4^{2-} is a similar tetrahedral oxoanion with PO_4^{3-}), the redox potential position, the firing procedure (firing is not done in the case of Cu modification), and the concentration of modified elements are candidate factors for this difference. The contribution of these factors to the activity difference between Cu and Mo modifications must be addressed in future studies.

Because molybdenum oxides possess a certain solubility against water, it is inappropriate to compare photocatalytic activity measurements using water purification. Moreover, the preparation of thin films using Mo-modified Ti-HAp powder with sufficient density, strength and repeatability onto the electrodes was not easy. Therefore, we have not conducted photocurrent experiments, but conducted PL and ESR measurements in this study to discuss the mechanism.

This study demonstrated that Mo modification is an effective strategy to enhance the photocatalytic activity of Ti-HAp. Results reported in the literature reveal that MoO_3 itself possesses antibacterial properties [50–53]. Therefore, this material might exhibit antibacterial and antivirus properties both in the dark and under UV illumination. Detailed investigations of this property will be undertaken in future studies.

4. Conclusions

For this study, we modified Ti-HAp with CaMoO_4 aqueous solution and evaluated UV light photocatalytic activity by the decomposition of gaseous IPA. After Mo modification, the crystal structure, morphology, light absorption, and specific surface area were almost identical. Small

(ca. 1 nm) clusters were observed on the surface of Mo-modified Ti-HAp. The Mo-modified Ti-HAp exhibited higher photocatalytic activity than Ti-HAp did. The photocatalytic activity of the Mo-modified samples increased concomitantly with increasing Mo concentration until 0.5% against Ti. Computer modeling indicated that MoO_4^{2-} doping into Ti-HAp structure plays no important role for activity increase. Results of ESR and PL analyses elucidated that the electron transfer from Ti 3d band to the MoO_x (Mo^{n+} ($n < 6$)) or Mo metallic cluster via wavefunction hybridization between the Ti 3d and the Mo 4d orbitals can suppress the recombination of photoinduced electron–hole pairs.

Acknowledgments

The authors are grateful to the staff of the Center of Advanced Materials Analysis (CAMA) at the Tokyo Institute of Technology for various characterizations and for helpful discussion related to this study. The authors thank Prof. Miyauchi, Dr. Yamaguchi, and Dr. Kishi for helpful discussion of this study.

Appendix A. Supplementary data

Supplementary material related to this article can be found, in the online version, at doi:<https://doi.org/10.1016/j.apcatb.2018.10.056>.

References

- [1] T. Kokubo, H.M. Kim, M. Kawashita, Novel bioactive materials with different mechanical properties, *Biomaterial* 24 (2003) 2161–2175.
- [2] B.M. Choudary, C. Sridhar, M.L. Kantam, G.T. Venkanna, B. Sreedhar, Design and evolution of copper apatite catalysts for N-arylation of heterocycles with chloro- and fluoroarenes, *J. Am. Chem. Soc.* 127 (2005) 9948–9949.
- [3] D.N. Misra, Adsorption from solutions on synthetic hydroxyapatite: nonaqueous vs. aqueous solvents, *J. Biomed. Mater. Res.* 48 (1999) 848–855.
- [4] Z.P. Yang, C.J. Zhang, Molecularly imprinted hydroxyapatite thin film for bilirubin recognition, *Biosens. Bioelectron.* 29 (2011) 167–171.
- [5] H. Nishikawa, K. Omamiuda, Photocatalytic activity of hydroxyapatite for methyl mercaptane, *J. Mol. Catal. A Chem.* 179 (2002) 193–200.
- [6] H. Nishikawa, Surface changes and radical formation on hydroxyapatite by UV irradiation for inducing photocatalytic activation, *J. Mol. Catal. A Chem.* 206 (2003) 331–338.
- [7] H. Nishikawa, A high active type of hydroxyapatite for photocatalytic decomposition of dimethyl sulfide under UV irradiation, *J. Mol. Catal. A Chem.* 207 (2004) 149–153.
- [8] T. Suzuki, T. Hatushika, Y. Hayakawa, Synthetic hydroxyapatites employed as inorganic cation exchangers, *J. Chem. Soc. Faraday Trans.* 77 (1981) 1059–1062.
- [9] X.B. Chen, J.V. Wright, J.L. Conca, L.M. Peurrung, Evaluation of heavy metal remediation using mineral apatite, *Water Air Soil Pollut.* 98 (1997) 57–78.
- [10] M. Tsukada, M. Wakamura, N. Yoshida, T. Watanabe, Band gap and photocatalytic properties of Ti-substituted hydroxyapatite: comparison with anatase-TiO₂, *J. Mol. Catal. A Chem.* 338 (2011) 18–23.
- [11] M. Wakamura, K. Hashimoto, T. Watanabe, Photocatalysis by calcium hydroxyapatite modified with Ti(IV): albumin decomposition and bactericidal effect, *Langmuir* 19 (2003) 3428–3431.
- [12] K. Kandori, M. Oketani, M. Wakamura, Decomposition of proteins by photocatalytic Ti(IV)-doped calcium hydroxyapatite particles, *Colloids Surf. B: Biointerfaces* 102 (2013) 908–914.
- [13] K. Kandori, T. Kurodam, M. Wakamura, Protein adsorption behaviors onto photocatalytic Ti(IV)-doped calcium hydroxyapatite particles, *Colloids Surf. B: Biointerfaces* 87 (2011) 472–479.
- [14] K. Kandori, M. Oketani, M. Wakamura, Effects of Ti(IV) substitution on protein adsorption behaviors of calcium hydroxyapatite particles, *Colloids Surf. B: Biointerfaces* 101 (2013) 68–73.
- [15] N. Yoshida, T. Ishida, C. Saiki, M. Wakamura, H. Osaki, K. Hashimoto, T. Watanabe, Preparation of transparent thin film of novel apatite-based photocatalyst, *Chem. Lett.* 34 (2005) 1666–1667.
- [16] A. Tsuruoka, T. Isobe, S. Matsushita, M. Wakamura, A. Nakajima, Comparison of photocatalytic activity and surface friction force variation on Ti-doped hydroxyapatite and anatase under UV illumination, *J. Photochem. Photobiol. A: Chem.* 311 (2015) 160–165.
- [17] M. Nakazawa, M. Yamada, M. Wakamura, H. Egusa, K. Sakurai, Activation of osteoblastic function on titanium surface with titanium-doped hydroxyapatite nanoparticle coating: an in vitro study, *Int. J. Oral Maxillofacial Implants* 32 (2017) 779–791.
- [18] M. Wakamura, Novel photocatalytic titanium apatite for environmental purification technology, *J. Soc. Inorg. Mater. Jpn.* 13 (2006) 516–519 [in Japanese].
- [19] Y. Gangarajula, R. Kedarnath, B. Gopal, Investigation of photocatalytic activity of pure strontium hydroxyapatite and its Ti-substituted and TiO₂ loaded forms, *Appl. Catal. A General* 506 (2015) 100–108.
- [20] Q. Li, X. Feng, X. Zhang, H. Song, J. Zhang, J. Shang, W. Sun, T. Zhu, M. Wakamura, M. Tsukada, Y. Lu, Photocatalytic degradation of bisphenol A using Ti-substituted hydroxyapatite, *Chinese J. Catal.* 35 (2014) 90–98.
- [21] M. Wakamura, H. Tanaka, Y. Naganuma, N. Yoshida, T. Watanabe, Surface structure and visible light photocatalytic activity of titanium-calcium hydroxyapatite modified with Cr(iii), *Adv. Powder Technol.* 22 (2011) 498–503.
- [22] M. Nishikawa, W.J. Yang, Y. Nosaka, Grafting effects of Cu²⁺ on the photocatalytic activity of titanium-substituted hydroxyapatite, *J. Mol. Catal. A Chem.* 378 (2013) 314–318.
- [23] H. Irie, S. Miura, K. Kamiya, K. Hashimoto, Efficient visible light-sensitive photocatalysts: grafting Cu(II) ions onto TiO₂ and WO₃ photocatalysts, *Chem. Phys. Lett.* 457 (2008) 202–205.
- [24] H. Irie, K. Kamiya, T. Shibanuma, S. Miura, D.A. Tryk, T. Yokoyama, K. Hashimoto, Visible light-sensitive Cu(II)-grafted TiO₂ photocatalysts: activities and X-ray absorption fine structure analyses, *J. Phys. Chem. C* 113 (2009) 10761–10766.
- [25] J. Herzfeld, R.G. Griffin, R.A. Haberkorn, Phosphorus-31 chemical-shift tensors in barium diethyl phosphate and urea-phosphoric acid: model compounds for phospholipid head-group studies, *Biochemistry* 17 (14) (1978) 2711–2718.
- [26] F.D. Hardcastle, I.E. Wachs, Determination of molybdenum-oxygen bond distances and bond orders by Raman spectroscopy, *J. Raman Spectrosc.* 21 (1990) 683–691.
- [27] R. Car, M. Parrinello, Unified approach for molecular dynamics and density-functional theory, *Phys. Rev. Lett.* 55 (1985) 2471–2474.
- [28] K. Prue thiaren, T. Isobe, S. Matsushita, J. Ye, A. Nakajima, Comparative study of photoinduced wettability conversion between [PW₁₂O₄₀]³⁻/brookite and [SiW₁₂O₄₀]⁴⁻/brookite hybrid films, *Matter. Chem. Phys.* 144 (2014) 327–334.
- [29] P.R. Harvey, R. Rudham, S. Ward, Photocatalytic oxidation of liquid propan-2-ol by titanium dioxide, *J. Chem. Soc. Faraday Trans. 1* (79) (1983) 1381–1390.
- [30] Y. Ohko, K. Hashimoto, A. Fujishima, Kinetics of photocatalytic reactions under extremely low-intensity UV illumination on titanium dioxide thin films, *J. Phys. Chem. A* 101 (1997) 8057–8062.
- [31] A. Mylonas, A. Hiskia, E. Androulaki, D. Dimotikali, E. Papaconstantinou, New aspect of the mechanism of photocatalytic oxidation of organic compounds by polyoxometalates in aqueous solutions. The selective photooxidation of propan-2-ol to propanone: the role of OH radicals, *Phys. Chem. Chem. Phys.* 1 (1999) 437–440.
- [32] S.A. Larson, J.A. Widgren, J.L. Falconer, Transient studies of 2-propanol photocatalytic oxidation on titania, *J. Catal.* 157 (1995) 611–625.
- [33] A. Fujishima, T.N. Rao, D.A. Tryk, Titanium dioxide photocatalysis, *J. Photochem. Photobiol. C* 1 (2000) 1–21.
- [34] W. Li, G.D. Meitzner, R.W. Borry III, E. Iglesia, Raman and X-ray absorption studies of Mo species in Mo/H-ZSM5 catalysts for non-oxidative CH₄ reactions, *J. Catal.* 191 (2000) 373–383.
- [35] M. Chen, U.V. Waghmare, C.M. Friend, E. Kaxiras, A density functional study of clean and hydrogen-covered α -MoO₃ (010): electronic structure and surface relaxation, *J. Chem. Phys.* 109 (1998) 6854–6860.
- [36] M. Oshikiri, J.H. Ye, M. Boero, Inhomogeneous RVO₄ photocatalyst systems (R = Y, Ce, Pr, Nd, Sm, Eu, Gd, Tb, Dy, Ho, Er, Tm, Yb, Lu), *J. Phys. Chem. C* 118 (2014) 8331–8341.
- [37] H. Monna, S. Ueno, T. Kanazawa, Properties of hydroxyapatite prepared by the hydrolysis of tricalcium phosphate, *J. Chem. Tech. Biotechnol.* 31 (1981) 15–24.
- [38] I. Nakamura, N. Neigishi, S. Kutsuna, T. Ihara, S. Sugihara, K. Takeuchi, Role of oxygen vacancy in the plasma-treated TiO₂ photocatalyst with visible light activity for NO removal, *J. Mol. Catal. A Chem.* 161 (2000) 205–212.
- [39] P.H. Kasai, Electron spin resonance studies of γ - and X-ray-irradiated zeolites, *J. Chem. Phys.* 43 (1965) 3322–3327.
- [40] J.H. Lunsford, ESR of adsorbed oxygen species, *Catal. Rev.* 8 (1973) 135–157.
- [41] Y. Nakaoka, Y. Nosaka, ESR Investigation into the effects of heat treatment and crystal structure on radicals produced over irradiated TiO₂ powder, *J. Photoch. Photobiol. A* 110 (1997) 299–305.
- [42] J.M. Coronado, A.J. Maira, J.C. Conesa, K.L. Yeung, V. Augugliaro, J. Soria, EPR study of the surface characteristics of nanostructured TiO₂ under UV irradiation, *Langmuir* 17 (2001) 5368–5374.
- [43] K.C. Khulbe, R.S. Mann, M. Ternan, Electron spin resonance studies of the surface chemistry of molybdenum-alumina catalysts, *Can. J. Chem.* 56 (1978) 1769–1772.
- [44] J. Liqiang, Y. Fulong, H. Haige, X. Baifu, C. Weimin, F. Honggang, Relationships of surface oxygen vacancies with photoluminescence and photocatalytic performance of ZnO nanoparticles, *Sci. Chin. B* 48 (2005) 25–30.
- [45] D. Aronov, A. Karlov, G. Rosenman, Hydroxyapatite nanoceramics: basic physical properties and biointerface modification, *J. Euro. Cer. Soc.* 27 (2007) 4181–4186.
- [46] Lange's Handbook of Chemistry 12th edition, Ed. J. A. Dean, McGraw-Hill Inc., New York, pp6–12 (1976).
- [47] Kagaku Binnran Third edition, Ed. The Chemical Society of Japan, Maruzen, Tokyo Japan, ppII–475 (1988) [in Japanese].
- [48] I.V. Kozhevnikov, Catalysis by heteropoly acids and multicomponent polyoxometalates in liquid-phase reactions, *Chem. Rev.* 98 (1998) 171–198.
- [49] Y. Nosaka, S. Takahashi, H. Sakamoto, A.Y. Nosaka, Reaction mechanism of Cu(II)-grafted visible-light responsive TiO₂ and WO₃ photocatalysts studied by using ESR spectroscopy and chemiluminescence photometry, *J. Phys. Chem. C* 115 (2011) 21283–21290.
- [50] C. Zollfrank, K. Gutbrod, P. Wechsler, J.P. Guggenbichler, Antimicrobial activity transition metal acid MoO₃ prevents microbial growth on material surfaces, *Mater. Sci. Eng. C* 32 (2012) 47–54.
- [51] M. Mizutani, K. Sunada, T. Isobe, S. Matsushita, A. Nakajima, Anti-bacterial and photocatalytic activities of (Mo_{0.5} W_{0.5})O₃ with Cu(Mo_{0.5} W_{0.5})O₄ prepared by impregnation method and mechanochemical processing, *J. Jpn. Soc. Colour Mater* 91 (3) (2018) 89–93.
- [52] K. Krishnamoorthy, M. Premanathan, M. Veerapandian, S.J. Kim, Nanostructured molybdenum oxide-based antibacterial paint: effective growth inhibition of various pathogenic bacteria, *Nanotechnology* 25 (2014) 315101(10pp).
- [53] C.C. Mardare, A.W. Hassel, Investigations on bactericidal properties of molybdenum-tungsten oxides combinatorial thin film material libraries, *ACS Comb. Sci.* 16 (2014) 631–639.